Evolution of Atmospheric Particles along Trajectories Crossing the Los Angeles Basin

L. S. HUGHES, J. O. ALLEN, P. BHAVE, M. J. KLEEMAN, AND G. R. CASS*

Environmental Engineering Science Department, MC 138-78, California Institute of Technology, Pasadena, California 91125

D.-Y. LIU, D. P. FERGENSON, B. D. MORRICAL, AND K. A. PRATHER

Department of Chemistry, University of California, Riverside, Riverside, California 92521

Trajectory analysis shows that the air masses arriving at Riverside, CA, on the afternoons of September 24 and 25, 1996, previously passed near air monitoring sites at Santa Catalina Island, Long Beach, and Fullerton, CA, in succession. At those sites, electrical aerosol analyzers and optical particle counters acquired continuous particle size distribution data, inertial impactor and bulk filter samples were taken with 4-h time resolution for determination of particle size and chemical composition during intensive sampling periods once per day at each site, and aerosol time-of-flight mass spectrometers acquired continuous data on particle size and composition at the single-particle level. These data permit particle evolution to be studied within single air masses as they sequentially pass several monitoring sites over a 2-day period. Air parcels associated with both of the trajectories studied show mineral dust, organic carbon, particulate nitrate and ammonium, and total suspended particulate matter concentrations that increase as transport occurs across the air basin. Large increases in particulate ammonium and nitrate concentrations occur between Fullerton and Riverside due to overnight air stagnation in an area with high gaseous ammonia emissions. The aerosol time-of-flight mass spectrometers show how the externally mixed population of individual particles is modified chemically during transport from Long Beach to Riverside, CA. The coastal aerosol at Long Beach containing sea-salt particles and primary carbon particles is changed substantially as these particles individually accumulate secondary ammonium nitrate and organics during travel across the air basin.

Introduction

The development of air quality models that assist communities in designing effective air quality control strategies depends on an understanding of the chemical and physical transformation processes that occur in the atmosphere. The study of such processes, however, is complicated by the movement of air masses; it is difficult to tell from data taken at fixed locations how and why particle evolution occurs. The ideal field study situation in many cases would be to move the air monitoring instruments, keeping them always within a single air parcel as it moves along a trajectory dictated by wind direction and speed in order to observe aerosol transformations as they happen. Unfortunately, the complexity of aerosol instruments and their power requirements often make such experiments impractical. Even instrumented aircraft have difficulty remaining aloft within the same air mass for several consecutive days. For that reason, few measurements exist showing how particle size distributions and chemical composition evolve in the urban atmosphere over a several day period within a single air parcel in the presence of atmospheric chemical reactions, dilution, and deposition.

In late September and early October 1996, a field experiment was conducted in southern California in which four air monitoring stations were located along a typical air parcel trajectory in an attempt to observe particle evolution within the same air mass as it passes over each of the four stations in succession (*1*). Particle size distribution, fine and total particle chemical composition, and size-segregated chemical composition measurements were taken sequentially at all four sites, at times intended to coincide with typical air mass motion, while continuous measurements of single-particle chemical composition also were made by aerosol time-of-flight mass spectrometry at three of the sites.

The purpose of this paper is to examine the resulting database for events in which air parcels meet the criterion of successive passes over two or more monitoring sites. Through this analysis, we develop a clear experimentally based picture of how particles and gases within the same air mass change over time during transit across the Los Angeles Basin.

Background

Studies of secondary particle formation processes have been carried out on a number of occasions in southern California by initializing a Lagrangian trajectory model with background pollutant concentration data taken upwind of the Los Angeles area and then comparing model predictions to pollutant measurements made on the downwind side of the city.

In one of the first of these studies, Roberts (*2*) examined SO_2(g) to particulate SO_4^{2-} conversion rates along air parcel trajectories stretching from the Pacific Coast inland to Pasadena, CA. From changes in the ratio of SO_2 to total airborne sulfur between the major SO_2 source areas at the coast versus measurements made at the downwind receptor site at Pasadena, it was calculated that SO_2 oxidation rates varied from 1 to 15% h^{-1}, depending on the event studied.

The formation of NH_4NO_3 aerosol within air parcels crossing the Los Angeles area was studied by Russell et al. (*3*). A photochemical trajectory model was used to predict total ammonium nitrate concentrations within air parcels arriving at El Monte, CA, at various times on June 28, 1974; the results were compared to field measurements taken at that site on that day by Reynolds et al. (*4*). Model predictions agreed well with measured particulate nitrate ion, ammonium ion, gas-phase ammonia, and ozone concentrations. A later version of this model (*5*) was used to examine air parcel trajectories that traversed southern California during a 2-day field study conducted in 1982 in which gas- and particle-phase nitrogen species, including NO, NO_2, HNO_3, NH_3(g), particulate NO_3^-, and particulate NH_4^+ were measured at 10

* Corresponding author present address: School of Earth and Atmospheric Sciences, Georgia Institute of Technology, Atlanta, GA 30332: phone: (404)894-3948; fax: (404)894-5638; e-mail: cass@eas.gatech.edu.

10.1021/es9908671 CCC: $19.00
Published on Web 06/29/2000

locations with 2- and 4-h time resolution (*6*). In this case, an air parcel trajectory was identified that passed over or near three monitoring sites in succession: Long Beach, Anaheim, and Rubidoux (a far-inland site near Riverside). This represents the only previous instance to date in which aerosol nitrate formation within the same air parcel has been observed at multiple points in time. These data are of particular value as a model verification tool, as the contents of the air parcel are well-known at several locations along the trajectory and initial conditions are well established.

Pandis et al. (*7*) examined sulfate production in the presence of an urban fog using several trajectory models applied to the database from the 1987 Southern California Air Quality Study (SCAQS) (*8*). These calculations sought to explain the elevated sulfate levels detected at inland sites downwind of an overnight fog that occurred at the Long Beach monitoring site. A model simulating only gas-phase chemical reactions was able to accurately predict aerosol sulfate concentrations within air parcels that had not passed through the fog, but sulfate concentrations within those air parcels that had passed through fog were underpredicted if only gas-phase chemical reactions were considered. A model that represented both gas- and aqueous-phase chemistry was able to account for the increased aerosol sulfate concentrations in air exposed to fog, shedding light on the heterogeneous chemical processes. In closely related work, sulfate and nitrate formation by heterogeneous processes along trajectories passing through stratus clouds have been studied by Seigneur and Wegrecki (*9*) modeling gas- and aqueous-phase data collected within clouds by Richards et al. (*10, 11*). The calculations included treatments of diffusion and vertical transport in addition to cloud chemistry, and good agreement was obtained with measured cloud species concentrations. Major nitrate formation pathways were found to be aqueous reduction of NO_3 radicals and heterogeneous hydrolysis of N_2O_5; major sulfate formation pathways were calculated to be aqueous oxidation of SO_2 by H_2O_2, O_2, and OH radicals.

Secondary organic aerosol formation along trajectories crossing southern California was studied by Pandis et al. (*12*). A photochemical trajectory model was applied to a summertime smog episode that occurred in Claremont, CA, on August 28, 1987. Calculations showed that approximately 18% of the organic aerosol burden at Claremont could be attributed to gas-to-particle conversion in the atmosphere.

Other recent studies combine these trajectory models for sulfate, nitrate, and secondary organic aerosol formation with emissions data on the size distribution of primary particle emissions from sources in order to render comprehensive predictions of the changes that occur in the size and chemical composition distribution of the atmospheric particle mixture (*13*−*17*). Models have been created both for internally mixed aerosols, in which all particles of the same size are assumed to have exactly the same composition (*13, 14, 16*), and for externally mixed aerosols that reflect the differences in initial particle chemical composition at different sources (*15, 17*). Predictions have been compared to cascade impactor measurements of ionic species, carbonaceous species, and mass size distributions taken in Claremont by Wall et al. (*18*) and by Zhang et al. (*19*).

In all cases except the study by Russell and Cass (*6*), only the particle characteristics at the end points of the trajectories studied have been known experimentally in any detail, and particle evolution along the trajectories has generally been inferred by calculations rather than actual observations. One purpose of the present research is to replace these inferences about the intermediate evolution of the particle size and composition distribution with actual measured values that can later be used for stringent tests of air quality model performance.

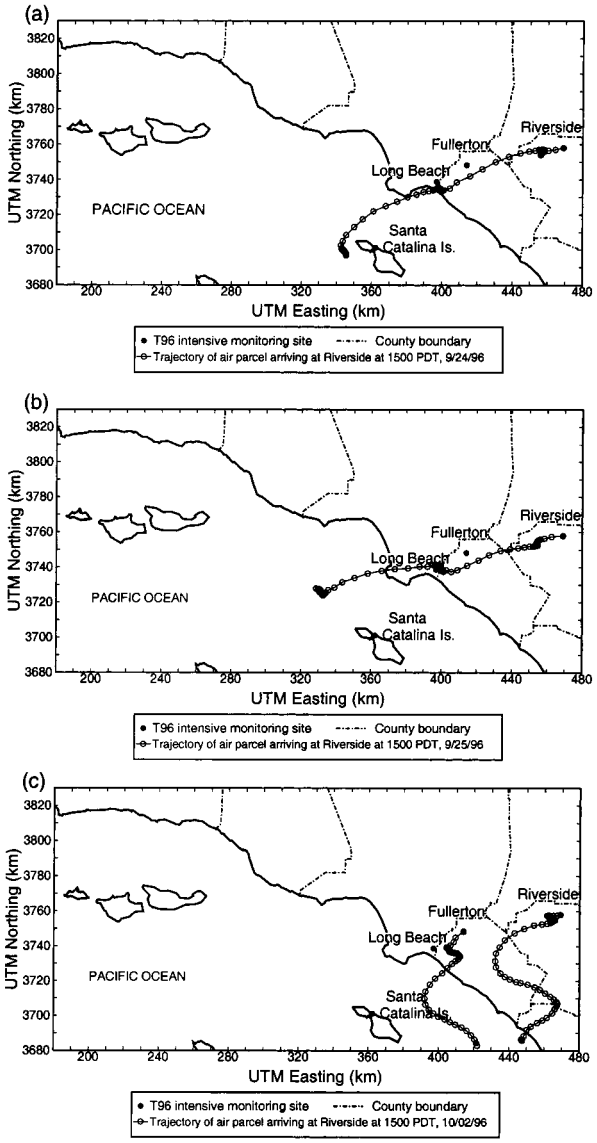

FIGURE 1. (a) Air parcel trajectory 1 reaching Riverside, CA, at 1500 h PDT on September 24, 1996. The trajectory passes near all three urban sampling sites and the background sampling site. Pattern is typical of the trajectories seen in the first week of sampling, September 23−30, 1996. (b) Air parcel trajectory 2 reaching Riverside, CA, at 1500 h PDT on September 25, 1996. (c) Air parcel trajectories reaching Fullerton and Riverside, CA, at 1500 h PDT on October 2, 1996. Both trajectories travel roughly northward and did not experience overnight stagnation on the night of September 30−October 1. This pattern is typical of the trajectories seen during the second week of sampling, October 1−3, 1996.

Experimental Methods

As part of the present study, ambient air samples were collected on 7 days over the course of 2 weeks in late September and early October 1996 (*1*). Instruments were stationed at three urban sites in the Los Angeles, CA, area chosen to lie along a seasonally typical air parcel trajectory: Long Beach, Fullerton, and Riverside. In addition, off-shore upwind background concentration data were taken at Santa Catalina Island (see Figure 1).

An electrical aerosol analyzer (EAA, TSI model 3030) and an aerosol time-of-flight mass spectrometer (ATOFMS) (*20, 21*) were operated continuously at each of the three urban sampling sites. Laser optical particle counters (OPCs, Particle Measuring Systems model ASASP-X) were operated continuously at the Long Beach and Riverside sites. The high-

TABLE 1. Intensive Sampling Time Periods

	Santa Catalina Island	Long Beach	Fullerton	Riverside
September 21−22, 1996	1300−1300 PDT[a]			
September 23, 1996		0700−1100 PDT	1100−1500 PDT	1500−1900 PDT
September 24, 1996		0700−1100 PDT	1100−1500 PDT	1500−1900 PDT
September 25, 1996				1500−1900 PDT
September 26, 1996				1500−1900 PDT
October 1, 1996		0700−1100 PDT	1100−1500 PDT	1500−1900 PDT
October 2, 1996		0700−1100 PDT	1100−1500 PDT	1500−1900 PDT

[a] PDT, Pacific Daylight Time.

resolution particle size distribution data taken by the electrical aerosol analyzers and optical particle counters are presented in refs *1* and *22*. A pair of micro-orifice cascade impactors (MSP Corp., model 110) and a low-volume filter-based fine and total suspended particle sampler (*1*) were operated at each urban site for a 4-h period of time on each day of the two 2-day periods of intensive sampling. Additional impactor and filter-based measurements were made at Santa Catalina Island (upwind of the other sites) on the days preceding the first intensive experiment, and at Riverside (at the downwind end of the air mass transport corridor) on the 2 days following the first intensive experiment, thus extending the first experiment to 6 days covering the period September 21−26, 1996. The second intensive experiment took place on October 1−2, 1996.

Background concentrations were measured for one 24-h period, starting at 1300 PDT September 21, 1996, at the University of Southern California's Philip K. Wrigley Marine Science Center near Two Harbors on Santa Catalina Island, 35 km upwind of the mainland. Three cascade impactors, two MOUDIs (MSP Corp., model 110) (*23*) with Teflon substrates, and one MOI (MSP Corp., model 110) with aluminum foil substrates were used at this location along with a modified low-volume filter sampler and a Dasibi (model 1003) ozone monitor.

The experimental apparatus and chemical analysis procedures are fully described by Hughes et al. (*1*). Impactor and filter samples were analyzed gravimetrically and by ion chromatography, colorimetry, thermal evolution and combustion analysis, and neutron activation analysis to measure the size distribution and ionic species, carbonaceous species, and trace elements distribution of the airborne particles over the period of these experiments. NO and NO_2 concentrations were measured continuously at the monitoring sites in Long Beach and Riverside (ThermoElectron Corp., model 14B/E); these data were supplemented by hourly NO and NO_2 data from nearby South Coast Air Quality Management District (SCAQMD) air monitoring sites. HNO_3 and NH_3 were measured with 4-h time resolution during intensive operating periods. HNO_3 was determined using the denuder difference method, and NH_3 was collected on an oxalic acid-impregnated filter downstream of a Teflon prefilter.

Total particulate mass, nitrate, and ammonium ion measurements made using Teflon filters were corrected for volatilization losses of fine particulate NH_4NO_3 during sampling. The volatilization loss of NO_3^- from each Teflon filter sample was determined by comparison to the fine particle NO_3^- collected simultaneously on a nylon filter located downstream of a MgO-coated diffusion denuder. The quantity of NO_3^- ion lost during sampling from the Teflon filter samples taken during this experiment averaged 4.8 $\mu g\ m^{-3}$ (range 0.11−12.7 $\mu g\ m^{-3}$). Correction for the volatilization losses was accomplished by adding a stoichiometrically equivalent amount of both NH_4^+ and NO_3^- to the values measured on all fine and total particle Teflon filter samples in an amount equal to the difference between the NO_3^- collection on the denuded nylon versus Teflon filters. NH_3(g) concentrations measured by collection on oxalic acid-impregnated filters downstream of Teflon particle prefilters likewise were corrected to subtract that portion of the NH_3(g) collected that was due to volatilization of NH_4NO_3 from the upstream Teflon prefilter.

NO, NO_2, and HNO_3 were not measured at Santa Catalina Island. PAN was not measured at any site during this study and is not included in the material balances presented later in this paper. Those PAN concentrations that have been measured in the Los Angeles area in recent years have been low, even during smog episodes; PAN measurements taken in late summer 1993 averaged only 0.92 ± 0.94 ppb in Long Beach, 1.06 ± 1.27 ppb in Central Los Angeles, and 1.76 ± 1.33 ppb in Azusa during a severe photochemical smog episode (*24*).

Four days (September 23 and 24, 1996, and October 1 and 2, 1996) were chosen for extensive sampling at the urban monitoring sites on the basis of weather predictions indicating probable inland air transport. Pairs of days were chosen for intensive experiments to accommodate the anticipated travel time of air parcels across the air basin (*5*). On these 4 days, the low-volume filter samplers and impactors at each site were used for one 4-h period each day (the "intensive operating period" or IOP). Intensive sampling was conducted at Riverside only on September 25 and 26, 1996, to observe the progression of air parcels sampled upwind on previous days.

The experiment was designed to permit a later search for "single air parcels" passing consecutively over several of our monitoring sites as they travel across the basin. Previous experience with experiments designed to achieve this objective (*5*) suggested the following time schedule: intensive sampling was conducted in Long Beach at 0700−1100 PDT, in Fullerton at 1100−1500 PDT, and in Riverside at 1500−1900 PDT. Sampling times and dates are summarized in Table 1.

Air parcel trajectories crossing southern California during the September 21−October 3, 1996, sampling period were calculated by backward integration through wind fields constructed according to the method of Goodin et al. (*25*). Meteorological data used as input to the trajectory calculations included hourly averaged wind speed and direction at 29 meteorological stations maintained by the South Coast Air Quality Management District.

Figure 1a−c illustrates characteristic air parcel trajectories occurring during the study. Each circle along the trajectories pictured in Figure 1 represents 1 h of elapsed time. The air parcel trajectories ending in Riverside at 1500 PDT on September 24 and on September 25, 1996, are shown in Figure 1, panels a and b, respectively. A similar on-shore wind pattern was seen throughout the period September 21−30, 1996. During that period, overnight stagnation occurred across the air basin every night for 15−18 h, beginning at about 1900−2200 PDT in the evening and ending at about 1200−1500 PDT the following day. Figure 1c shows the calculated air parcel trajectories ending at the Fullerton and Riverside air monitoring sites at 1500 PDT on October 2, 1996. Instead

of the overnight stagnation seen the previous week, air flowed up the coast from the southeast overnight. Air parcels during that second phase of the experiment did not travel along a direct eastward inland route that would cause them to pass over more than one of the three established urban monitoring sites, and for that reason the October 1−2, 1996, intensive experiment will not be discussed further here.

Of the days that included data from all three urban sites, the closest match to the desired transport conditions occurred over the period September 21−24, 1996 (trajectory 1), shown in Figure 1a. Back-calculation of the trajectories from Riverside indicates that the air that arrived in Riverside over the period 1500−1900 PDT September 24, 1996, originated near Santa Catalina Island during the September 21−22 background concentration measurement experiments, stagnated in and near the Long Beach monitoring site over the night and throughout the morning of September 23, 1996 (IOP 0700−1100 PDT), and passed through Fullerton at 1400−1700 PDT September 23, 1996 (IOP 1100−1500 PDT). Similar transport conditions continued during the period September 24−25, 1996 (trajectory 2), producing another air parcel trajectory, shown in Figure 1b, which passed near each monitoring site in succession. The air mass that arrived in Riverside during intensive sampling at 1500−1900 PDT on September 25, 1996, passed through Fullerton at 1430−1900 PDT September 24, 1996 (IOP 1100−1500 PDT), and stagnated in and near the Long Beach monitoring site over the night and throughout the morning of September 24, 1996 (IOP 0700−1100 PDT).

The remainder of this paper will examine the evolution of the air masses as they travel along these two trajectories, passing over each of three or four sampling sites in succession.

Results and Discussion

Material balances on the nitrogen-containing pollutants measured sequentially along the two air parcel trajectories studied have been constructed, as shown in Figure 2. All concentrations are shown in terms of μg of nitrogen m^{-3}. Figure 2a shows the nitrogen species mass balance along the September 21−24, 1996, trajectory; Figure 2b shows the same data for the September 24−25, 1996, trajectory.

The total aerosol ammonium plus nitrate concentration begins at a very low value of 1.8 μg of N m^{-3} over the ocean at Santa Catalina Island. While HNO_3 was not measured at Santa Catalina Island during this study, previous work shows that HNO_3 concentrations over the ocean upwind of Los Angeles at San Nicolas Island (see Figure 1) are very low, averaging about 10% of fine aerosol nitrate concentrations (*26*). As the trajectory 1 air parcel stagnates near Long Beach in the morning hours of September 23, substantial quantities of NO, and to a lesser extent NO_2, accumulate within the air mass studied due to combustion source emissions within the urban area. The ammonium plus nitrate nitrogen concentration in the particle phase more than doubles to a total of 4.7 μg of N m^{-3} at Long Beach. Gas-phase nitric acid levels at Long Beach remain negligible; instead, nitric acid formed is apparently quickly transferred to the particle phase or removed by dry deposition. The trajectory 2 air mass measured in Long Beach likewise shows elevated quantities of NO, NO_2, and particulate ammonium and nitrate in the presence of a negligible HNO_3 concentration.

Over the course of a few hours transit from Long Beach to Fullerton, NO conversion to form more NO_2 is observed, accompanied by small but noticeable increases in nitric acid vapor and increased gaseous ammonia concentrations. Higher HNO_3 and NH_3 concentrations can be maintained in the gas phase at Fullerton in the midday period, as ambient temperatures are higher there than at Long Beach during the earlier hours of the day (see refs *27* and *28*). In the trajectory 1 air mass, particulate ammonium and nitrate

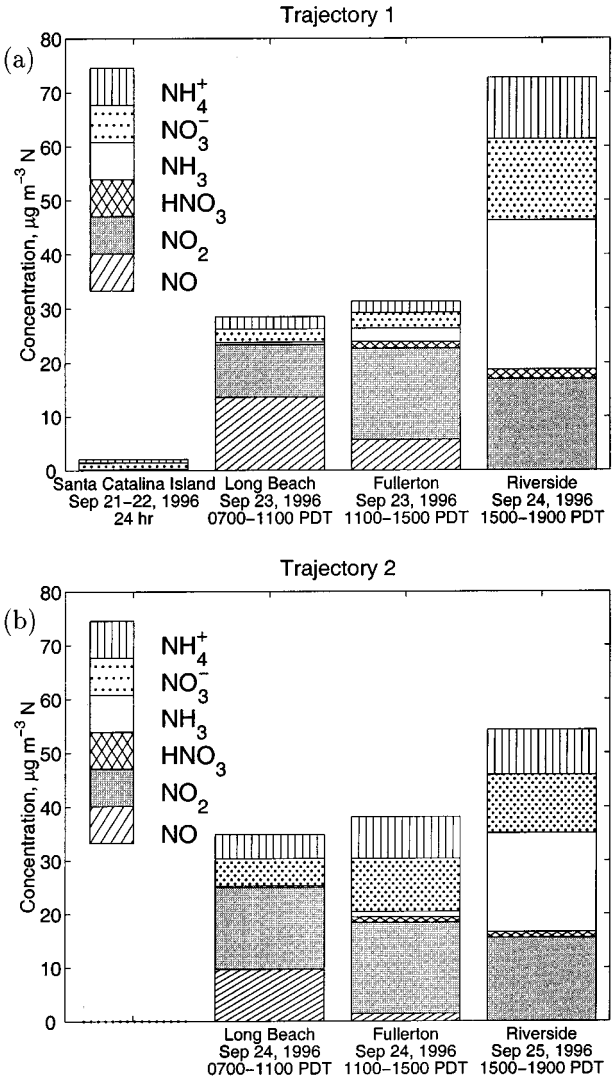

FIGURE 2. (a) Nitrogen species balances along trajectory 1, September 21−24, 1996. NO, NO_2, and HNO_3 were not measured at Santa Catalina Island. (b) Nitrogen species balances along trajectory 2, September 24−25, 1996.

concentrations at Fullerton remain about the same as were observed earlier at the Long Beach site, indicating that dilution and dry deposition have compensated for emissions and pollutant transformation between Long Beach and Fullerton. In the trajectory 2 air mass, particulate ammonium and nitrate concentrations at Fullerton are nearly double those at Long Beach.

After passing Fullerton, the air parcels studied pass over western San Bernadino County and then stagnate in western Riverside County overnight. By the following afternoon, as each air parcel finally reaches Riverside, essentially all NO has been converted to NO_2, and approximately half of the oxides of nitrogen in each air parcel exist as inorganic nitrates (HNO_3 plus aerosol NO_3^-) formed from the further oxidation of NO_2.

Even more remarkably, as each of the two air parcels studied reaches Riverside, about half of the measured reactive nitrogen exists as NH_3 gas plus aerosol NH_4^+. This large amount of ammonia plus ammonium ion accumulated in the air parcel as it passed over the agricultural areas in western San Bernadino and Riverside Counties. Emissions inventories and air quality modeling studies identify 54 types of ammonia emissions sources in the Los Angeles area, some of the largest of which are dairy farms, other livestock waste decomposition,

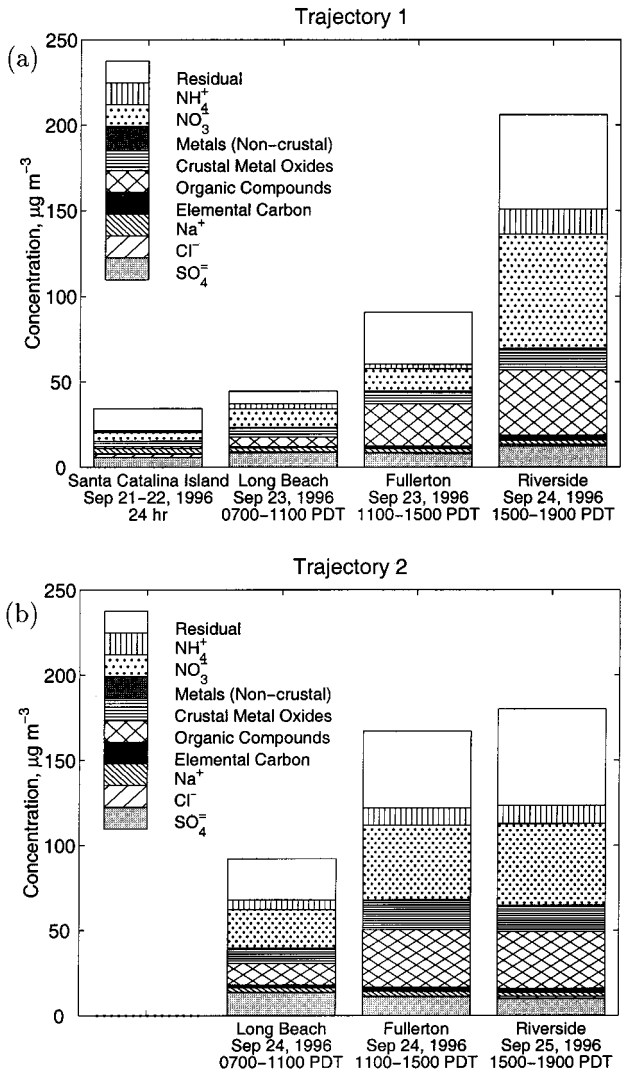

FIGURE 3. (a) Total suspended particulate concentrations and chemical compositions along trajectory 1, September 21−24, 1996, and (b) along trajectory 2, September 24−25, 1996.

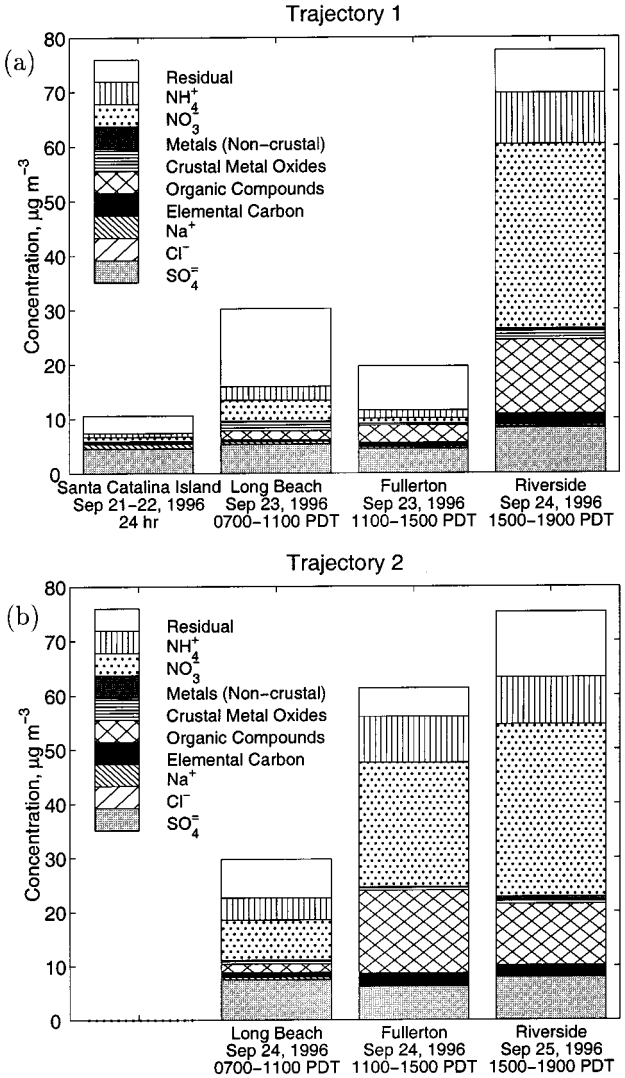

FIGURE 4. Fine particle ($D_a < 1.8\ \mu$m) concentrations and chemical compositions (a) along trajectory 1, September 21−24, 1996, and (b) along trajectory 2, September 24−25, 1996.

and fertilizer use in these agricultural areas (*3, 5, 17, 29*). As NH_3 emissions into the air parcels increase, both the NH_3 and the inorganic nitrate formed from NO_2 oxidation react to form particle-phase NH_4NO_3. HNO_3 concentrations are depleted due to aerosol NH_4NO_3 production, dilution, and dry deposition, while a substantial excess of NH_3 gas still exists in each air parcel at the end of the second day of transport across the air basin despite the foregoing dilution, transformation, and removal processes.

Material balances on the bulk chemical composition of total suspended particulate matter (TSP) concentrations and fine particle (particle diameter $D_a \leq 1.8\ \mu$m) concentrations constructed from chemical analysis of filter samples are shown in Figures 3 and 4, respectively. Material balances on the trajectory 1 air mass are presented in Figures 3a and 4a; material balances on the trajectory 2 air mass are presented in Figures 3b and 4b. In compiling the mass balances in this study, organic compound concentrations are estimated by multiplying organic carbon concentrations by a factor of 1.4 to account for the mass of H, O, N, and S in the organic compounds (*30*). Metals are presented at the equivalent mass concentrations of their common oxides. "Residual" concentrations indicate the gravimetrically determined mass fractions that are not accounted for by identified chemical components. A portion of this unidentified material undoubtedly includes silicate minerals and calcium-containing mineral matter that were not measured by neutron activation analysis in this experiment. An ion balance was constructed on the ionic species present in each of the filter samples. The data show that ion balances on average close to within ±15% for fine particle samples and within ±21% for TSP samples. The measurements made at Riverside generally show an excess of identified anions over identified cations.

Airborne particle mass concentrations within both trajectory air parcels increase during transport across the air basin, with the highest particle levels present at Riverside. Sulfate ion concentrations of about 5.8 μg m^{-3} observed upwind of the urban area at Santa Catalina Island do not increase greatly as the trajectory 1 air parcel passes over the first two urban sites. Even though there is a large amount of fuel combustion in Los Angeles, especially in the Long Beach harbor industrial and petroleum refining area, local sulfur oxide emissions have been driven to very low levels through the use of gaseous fuels and strict controls on industrial processes (*31, 32*). Similarly, the sulfate ion concentration does not increase with distance traveled across the basin as the trajectory 2 air parcel passes over the three urban monitoring sites. This confirms that there are few primary sulfate sources in the area today and that little SO_2 to sulfate conversion occurred in the atmosphere during these experiments. Sodium con-

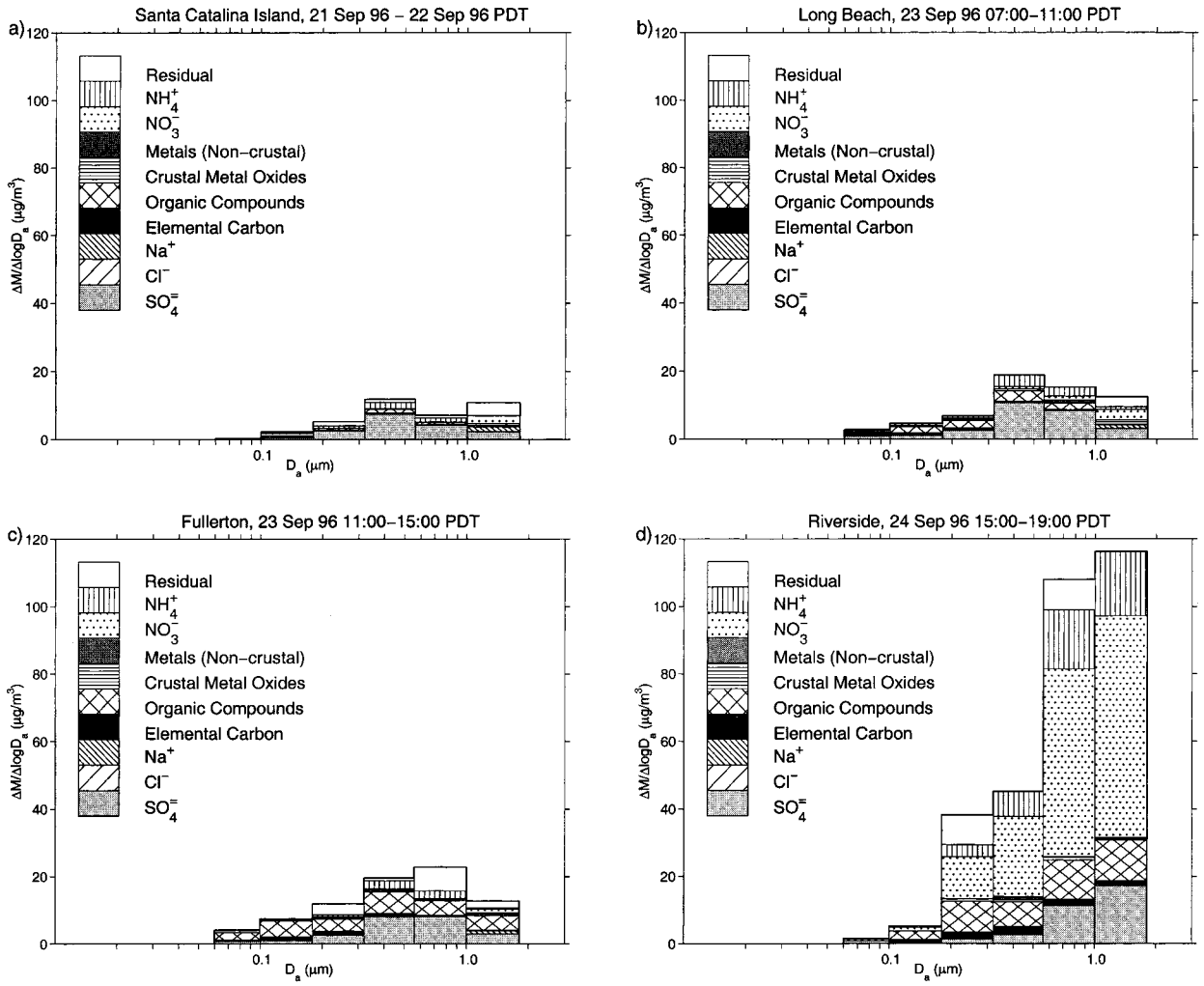

FIGURE 5. Size-dependent chemical compositions along trajectory 1, September 21−24, 1996. (a) Santa Catalina Island, September 21−22, 1996; (b) Long Beach, September 23, 1996, 0700−1100 h PDT; (c) Fullerton, September 23, 1996, 1100−1500 h PDT; (d) Riverside, September 24, 1996, 1500−1900 h PDT. Particle sizes are given as aerodynamic diameters.

centrations within both trajectory air parcels decline slightly while traveling inland from the coast, an indication that sea salt is the only significant sodium source.

Mineral dust (TSP crustal metal oxides), elemental carbon, and organic compound concentrations increase in the trajectory 1 air parcel during transport across the air basin. The increases are modest between Long Beach and Fullerton and much larger between Fullerton and Riverside, reflecting the longer travel times and greater emissions between Fullerton and Riverside and the generally drier and dustier soil conditions in the Riverside area when compared to the near coastal plain. Most dramatically, ammonium plus nitrate concentrations in the fine particle fraction of the aerosol reach $42.0 \pm 3.7\ \mu g\ m^{-3}$ at Riverside on September 24, which is over 15 times higher than the fine particle ammonium plus nitrate concentrations measured in Fullerton the day before. The high ammonium and nitrate concentrations at the end of trajectory 1 in Riverside are accompanied by $12.6 \pm 4.1\ \mu g\ m^{-3}$ of fine particle organic compounds, yielding overall fine particle concentrations of $77.6 \pm 5.8\ \mu g\ m^{-3}$. TSP concentrations exceeded $200\ \mu g\ m^{-3}$ at Riverside at the end of air parcel trajectory 1.

In contrast to events that occurred the previous day along trajectory 1, mineral dust, organic compounds, and particulate ammonium plus nitrate concentrations within the trajectory 2 air parcel increased significantly during transit between Long Beach and Fullerton. The largest part of the mass increase occurred due to ammonium nitrate production. Fine particle ammonium and nitrate increased by nearly a factor of 3 between Long Beach and Fullerton on September 24. The nitrogen balance in Figure 2 shows an earlier conversion of NO to NO_2 during the trajectory 2 event when compared to the trajectory 1 event, which may be responsible for the more rapid production of aerosol nitrate along trajectory 2. Production of ammonium nitrate during travel between Long Beach and Fullerton requires ammonia emissions into the air parcel. Small but numerous ammonia sources exist on the western side of the air basin (*3, 5, 17, 29*), including recently documented emissions from motor vehicle traffic (*33*). The fine particle ammonium and nitrate concentrations within the trajectory 2 air mass continue to increase across the basin, reaching $40.5 \pm 3.5\ \mu g\ m^{-3}$ at Riverside on September 25, which accounts for more than half of the overall fine particle concentration of $75.3 \pm 4.8\ \mu g\ m^{-3}$ at the end of trajectory 2.

The size-dependent chemical composition of the fine fraction of the aerosol during each intensive sampling period was determined through analysis of cascade impactor samples. The size-segregated chemical compositions during the four observations taken along the trajectory 1 air parcel path of September 21−24, 1996, are shown in Figure 5; the size-segregated chemical compositions of the samples taken along the trajectory 2 air parcel path of September 24−25, 1996, are shown in Figure 6. Comparison of fine particle

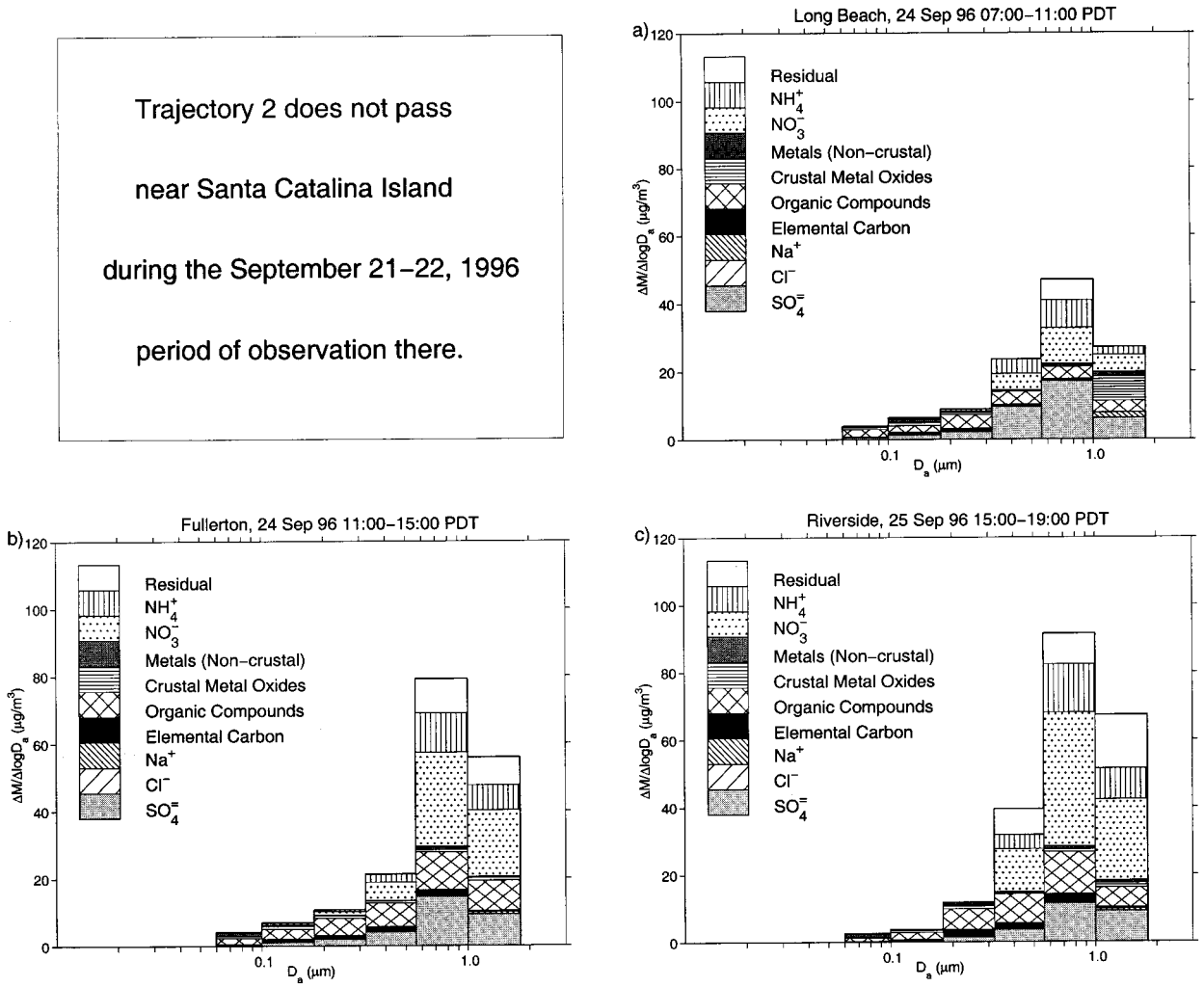

FIGURE 6. Size-dependent chemical compositions along trajectory 2, September 24−25, 1996. (a) Long Beach, September 24, 1996, 0700−1100 h PDT; (b) Fullerton, September 24, 1996, 1100−1500 h PDT; (c) Riverside, September 25, 1996, 1500−1900 h PDT. Particle sizes are given as aerodynamic diameters.

filter samples to the summation of the impactor stages shows agreement on average to within ±10% for EC, SO_4^{2-}, and NH_4^+; within ±15% for NO_3^-; and within ±25% for organic carbon. The impactor samples are higher than the filters for EC and sulfate and lower than the filters for organic carbon and the more volatile NH_4^+ and NO_3^-, thus suggesting some NH_4NO_3 evaporation from the impactors. Generally, the integrated impactor results and the fine filter results for a single sampling event are statistically indistinguishable from each other, given the analytical uncertainties.

The trajectory 1 air parcel shows a large increase in aerosol mass concentration and a shift in the particle size distribution to larger sizes during transport from Fullerton to Riverside. This can occur due to preferential growth of secondary aerosol ammonium nitrate on the hygroscopic non-sea-salt background aerosol particles that are present initially with a peak concentration at the larger end of the accumulation mode (*35*). Changes in particle size within the trajectory 2 air parcel are explained in detail by Kleeman et al. (*17, 35*).

Chemical differences between the particles at Long Beach versus Santa Catalina Island include an increase in organic carbon, elemental carbon, and aerosol nitrate in submicron-size particles at Long Beach. The Long Beach aerosol also shows increases in such trace elements as Zn, Al, and Fe when compared to Santa Catalina Island. Several other observations can be made that show evidence of chemical transformations occurring in the course of transport across the air basin. The Na concentration and size distribution is very similar at both Santa Catalina Island and Long Beach, which would be expected since the primary source of Na at both locations is the same (i.e., sea salt). Aerosol chloride concentrations at Long Beach on September 23 are much lower than at Santa Catalina Island, and the majority of the aerosol NO_3^- at Long Beach is seen in Figure 5b to be associated with the largest impactor bin that also contains the bulk of the aerosol Na. All of this is consistent with air quality models that predict Cl^- displacement by NO_3^- due to atmospheric chemical reaction in the particle phase, as has been confirmed previously by analysis of single-particle composition data taken during this experiment at Long Beach (*36*). If HNO_3 reacts with NaCl, then HCl is liberated from the particle phase and accumulates in the gas phase (*37*). Though aerosol-phase Cl^- virtually disappears from the air parcel by the time that it is sampled in Fullerton, aerosol Cl^- concentrations comparable to those seen at Santa Catalina Island are observed further along the trajectory in Riverside. (Cl^- concentrations are of a scale too small to be seen in Figures 5 and 6.) The renewed presence of Cl^- in aerosol form suggests that elevated levels of NH_3(g) in Riverside (see Figure 2) may react with high concentrations of gaseous HCl to produce particulate NH_4Cl (*37*). The equilibrium dissociation constant for ammonium chloride is very sensitive to temperature and relative humidity. Over the range of temperature and relative humidity conditions measured

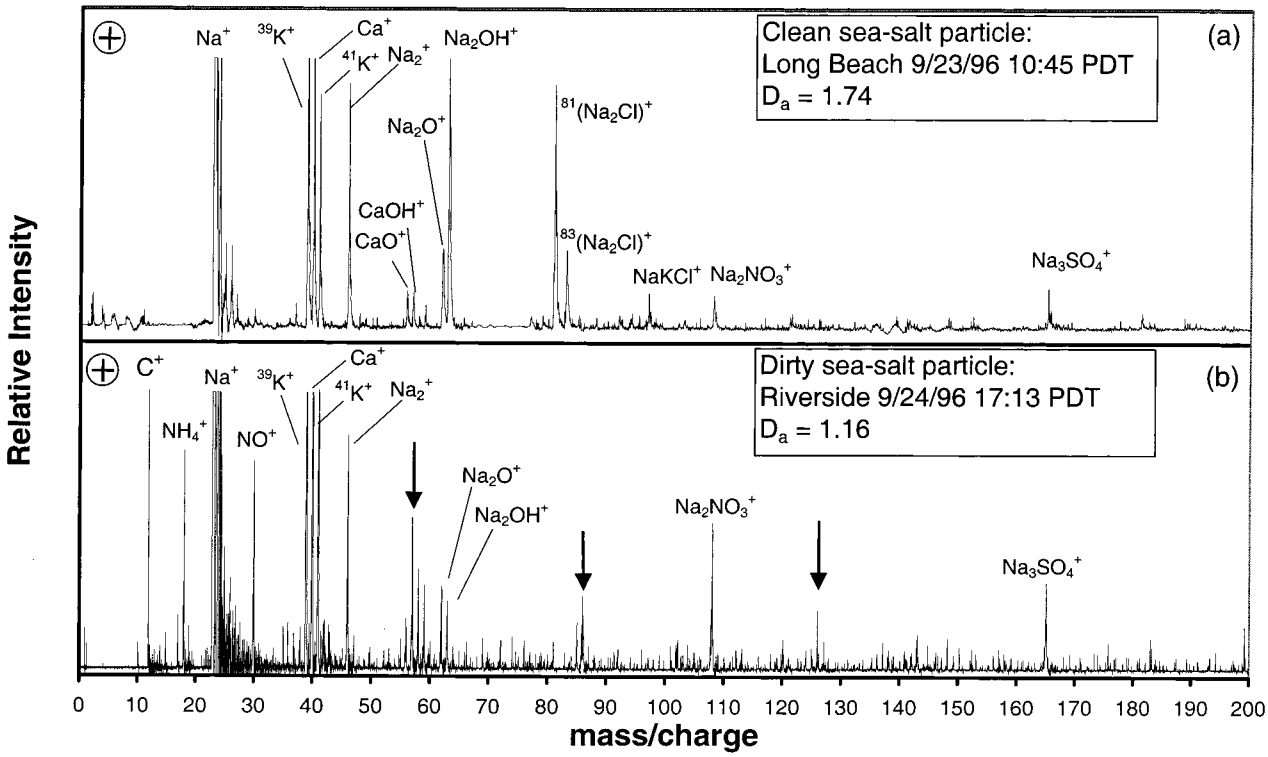

FIGURE 7. (a) Representative ATOFMS spectrum of a "clean" sea-salt particle observed in Long Beach. (b) Representative ATOFMS spectrum of a "dirty" sea-salt particle arriving in Riverside that has been transformed by gas-to-particle conversion processes.

during the intensive sampling period on September 24 at Riverside, 24 °C and 61% RH to 35 °C and 33% RH, the concentration product [HCl][NH_3] at equilibrium with solid-phase ammonium chloride falls in the approximate range of 56−725 ppb^2, according to the data of Pio and Harrison (*38*). Over the range of temperature and relative humidity conditions measured during the intensive sampling period on September 25 at Riverside, 21.5 °C and 67.5% RH to 32 °C and 37.5% RH, the equilibrium concentration product [HCl]-[NH_3] falls in the range of 31−368 ppb^2.

HCl was not measured in this study; NH_3 was measured with 4-h time resolution during the intensive sampling period. Measured NH_3 concentrations on the 2 days indicate that for solid-phase NH_4Cl to be in equilibrium with gas-phase concentrations at some time within the intensive sampling period, HCl concentrations would need to reach at minimum about 1.17 and 0.96 ppb on September 24 and 25, respectively. Measurements in Riverside (Rubidoux) in September and October 1986 found daily average HCl concentrations of 0.25−1.0 ppb (*37*), suggesting that conditions necessary for the presence of some solid-phase NH_4Cl in equilibrium with gas-phase NH_3 and HCl could reasonably have been present during the intensive sampling periods of September 24 and 25.

The ATOFMS instruments, operated continuously in positive ion mode at the Long Beach and Riverside sampling sites, provide measurements of the chemical composition and size of individual aerosol particles at the beginning and end of the two air parcel trajectories studied here. At the time this study was carried out, the ATOFMS instruments could produce either a positive or a negative ion spectrum for each particle hit by the mass spectrometry ablation laser. The choice was made to collect positive ion data throughout this study, and so the negative ion markers for sulfate ion species were not available. Modifications to the transportable ATOFMS instruments since the close of this study have added dual ion detection capability, and future studies will have both a positive and a negative ion spectrum for each hit particle.

The mass spectra of the individual particles analyzed during the 4-h impactor sampling periods at the start and end of each trajectory were gathered together and compared to describe the changes that occur at the single-particle level as air masses move across the air basin. Figure 7 illustrates the type of comparisons that can be made at the single-particle level. Figure 7a shows the mass spectrum of a clean sea-salt particle of 1.74 μm aerodynamic diameter sampled at Long Beach on the morning of the first day of trajectory 1. The spectrum is characterized by large sodium (Na^+, NaO^+, and Na_2OH^+) peaks with the strong presence of that sodium as NaCl (see Na_2Cl^+ ion peaks) and minor amounts of sodium nitrate ($NaNO_3^+$ marker ion) and sodium sulfate ($Na_3SO_4^+$ ion). Calcium and potassium also are present in sea salt and are easily seen in the mass spectrum of the clean sea-salt particle. Figure 7b illustrates the changes that such a particle undergoes during transport from Long Beach to Riverside over approximately a 1.5-day period. The dirty sea-salt particle at Riverside is still identified by its very large sodium marker content. This aged sea-salt particle has been completely stripped of its chloride content by atmospheric chemical reactions involving the oxides of nitrogen to form sodium nitrate (see loss of mass 81 and 83 Na_2Cl^+ peaks accompanied by increase in the magnitude of the $Na_2NO_3^+$ peak). This can occur by the heterogeneous reaction of sea salt with vapor-phase HNO_3 to form particulate $NaNO_3$ while releasing HCl gas (*36*, *37*); there are a number of other routes by which such conversion can occur as well (*39*−*42*). Further, the dirty sea-salt particle arriving at Riverside has accumulated gas-to-particle conversion products in the form of ammonium (NH_4^+) and nitrate (NO^+ marker) additions plus a coating of organic carbon compounds (C^+ marker, as well as yet unidentified mass fragments at the locations of the arrows in Figure 7b that are often seen in the mass spectra of organic aerosol particles). The dirty sea-salt particle shows almost exactly the combination of species predicted by Kleeman and Cass (*17*) through air quality modeling calculations for an aged sea-salt particle of 1.61 μm diameter transported across the Los Angeles Basin and arriving at

Claremont, CA, in August 1987 (sodium with lesser amounts of ammonium combined with nitrate; complete chloride removal; traces of organics and sulfates, plus other elements, e.g., K, Ca, etc.).

Changes in the aerosol population as air masses are transported across the Los Angeles basin can be summarized based on analysis of the thousands of separate particles sampled by the ATOFMS systems during the 4-h periods at the start (Long Beach) and at the end (Riverside) of trajectories 1 and 2. Statistically large numbers of particles were sampled over the size range of 0.32−3.5 μm aerodynamic diameter at Riverside and over the range of 0.56−3.5 μm at Long Beach. Particles at the larger end of this size range are most easily detected and sampled by the ATOFMS systems. To correct for this decline in particle detection efficiency with decreasing particle size, the counting efficiencies of the ATOFMS systems were determined by comparison with simultaneous measurements of the atmospheric particle number distribution and mass distribution made during this experiment by laser optical particle counters and micro-orifice impactors as described by Allen et al. (*22*). Using the resulting detection efficiency curves extrapolated upward to 3.5 μm particle diameter, each particle for which a mass spectrum was obtained was "duplicated" in proportion to the degree to which particles of that size are undercounted by the ATOFMS systems. This process results in a collection of particles present at the start and end of each trajectory whose number concentration as a function of size matches that of the atmosphere at the time of sampling; each particle has a chemical composition represented by its mass spectrum.

The major chemical substances present in each particle were then summarized based on the presence of key indicator ions in the ATOFMS mass spectra. These key indicator ions are mass 18 for ammonium (detected as NH_4^+); mass between 22 and 23.5 for sodium (detected as Na^+); mass 30 (NO^+) or mass 108 ($Na_2NO_3^+$) for nitrate ion; mass 12 (C^+), 36 (C_3^+), or 37 (C_3H^+) for carbon; and masses 27 (Al^+) and 56 (Fe^+/CaO^+) or mass 7 (Li^+) as indicative of mineral dust particles. Occasionally a particle that produces H^+ counts (between masses 0.5 and 2.5) that go offscale (greater than 10 000 arbitrary units) is identified as a dust particle based on similar and unique behavior seen during source tests applied to local soil samples. A peak that corresponds to one of these key ions is judged to be present in the mass spectrum of a particle if peak height and peak area equal or exceed 10 and 15 arbitrary units, respectively, for the laboratory-based instrument at Riverside or 15 and 30 arbitrary units, respectively, for the transportable instrument at Long Beach (the instrument designs are slightly different; these criteria provide comparable detection thresholds). To exclude consideration of trace amounts of a substance, the key ions are considered when classifying a particle only if their peak area exceeds 0.5% of the total peak area of the particle's mass spectrum. When the target masses listed above give unusually large signal, the base area of the peak for masses 23, 27, and 56 is broadened to the ranges 22−24, 25−29 and 54−58 mass units as long as the peak area is greater than or equal to 2500 arbitrary units. The range for mass 7 is broadened to 5−9 mass units as long as the peak area is greater than or equal to 200 arbitrary units. Since a positive ion indicative of the sulfate content of ammonium sulfate particles is not available, sulfate-containing aerosols cannot be enumerated in this study. Particle spectra were classified according to the presence or the absence of only these five key indicator ion groups; particles may contain other substances that were not specifically considered in this analysis. Particles were separated into particle size intervals that correspond to those of the impactor bins, and all particles having the same combination of key indicator ions within each size interval were grouped together. The results of this grouping of particles by type and size are pictured in Figure 8.

Figure 8 provides a color-coded display that shows for the first time a counting efficiency-corrected description of the extent of external mixing of major chemical substances in the atmospheric aerosol as a function of particle size. In addition, the figure demonstrates how the particle population changes due to dilution, deposition, emissions of new particles, and gas-to-particle conversion processes as the same air parcel moves across the Los Angeles urban area. Each of the squares in Figure 8 contains 100 colored dots, and each dot represents 1% of the number of particles in the atmosphere within the indicated size range. A dot having only a single color represents a comparatively simple particle type containing predominantly one of the key marker ions: blue for sodium-containing, red for nitrate-containing, orange for carbon-containing, or gray for mineral dust-containing particles. A dot with stripes of more than one color represents a group of more complex particles whose spectra contain more than one of the key marker substances. The color coding is a qualitative indicator of the composition of these complex particles; no statement is made about the mass fraction of each substance within the particles of that group. In particular, since the sensitivity of the ATOFMS for Na^+ is 71 times greater than for NH_4^+ (*43*), it is possible for a particle that contains mostly sea salt with a small quantity of ammonium nitrate to produce a mass spectrum with such a small NH_4^+ peak that it would be recorded as a sodium-only particle. Therefore, the reader should not interpret the solid blue and orange dots as denoting only pure sea-salt or carbon particles, respectively, but rather particles that produced spectra dominated by sodium and carbon peaks; there could be small quantities of gas-to-particle conversion products present on those particles at concentrations below the quantification limits used here. A blue and red striped dot represents a group of sodium nitrate-containing particles (e.g., wholly or partly reacted sea-salt aerosol). A yellow and red striped dot represents a population of ammonium nitrate-containing particles. Dots that contain only orange (carbon) and yellow (ammonium) stripes could well indicate a group of particles with both carbon and ammonium sulfate, as the sulfate content of the particle would not be detected in this experiment. All combinations of key indicator ions that are present in greater than 0.5% of the particles in a given size range (a value which rounds up to a whole dot) are shown by appropriate stripe patterns in Figure 8. Particle types that individually account for less than 0.5% of the particle population in a given size range are grouped together and represented by a green dot or dots.

Some atmospheric particles are simple representatives of the direct emissions from a primary particle source type. Carbon-containing particles are emitted from many primary pollution sources, and an unreacted sea-salt particle would be classified solely as a sodium-containing particle under this classification scheme. As these primary particle types interact with gas-phase air pollutants during transport across the air basin, the primary particles begin to incorporate secondary reaction products and become more complex. For example, sea-salt particles can react with the oxides of nitrogen in the atmosphere to produce sodium nitrate aerosol, which would be described as sodium- and nitrate-containing particles (blue and red striped dot). Primary carbon particles could acquire a coating of secondary ammonium nitrate, becoming a mixed carbon/ammonium/nitrate aerosol (orange, yellow, and red striped dot).

The left column of Figure 8 represents the overall population of particles sampled in the morning of September 23 at Long Beach at the start of trajectory 1. In the largest particle size range examined, 14% of the particles present at Long Beach produced spectra with quantifiable amounts of sodium or sodium chloride markers (blue only) but not sodium

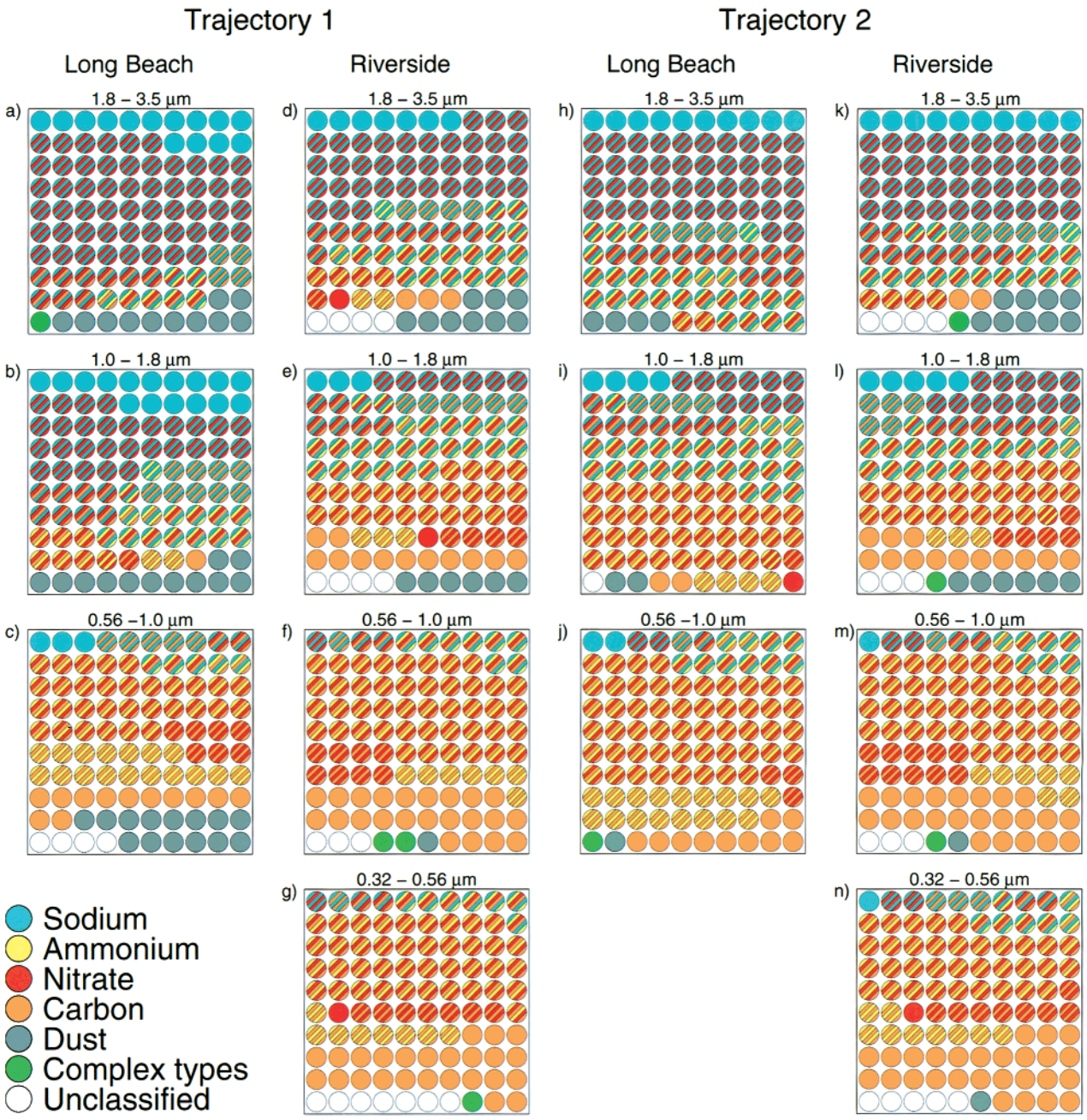

FIGURE 8. Chemical compositions of size-segregated particle populations at the start and end of trajectories 1 and 2 as measured by the ATOFMS instruments. Each dot represents 1% of the particle population within the indicated aerodynamic particle diameter range. (a–c) Particle populations at the beginning of trajectory 1, Long Beach, September 23, 1996, 0700–1100 h PDT. (d–g) Particle populations at the end of trajectory 1, Riverside, September 24, 1996, 1500–1900 h PDT. (h–j) Particle populations at the beginning of trajectory 2, Long Beach, September 24, 1996, 0700–1100 h PDT. (k–n) Particle populations at the end of trajectory 2, Riverside, September 25, 1996, 1500–1900 h PDT.

nitrate, indicating largely unreacted sea-salt particles. Sodium nitrate was present in most of the remaining particles sampled in the largest size range studied, indicating that a partial conversion of sodium chloride to sodium nitrate was underway at this time at Long Beach. Trajectory analysis shows that the air parcel sampled at Long Beach during the period 0700–1100 PDT on September 23 had been over land or over the very busy Long Beach Harbor area since about 1600 PDT on September 22 (see Figure 1a). Carbon, ammonium, and mineral dust also are detected in a small percentage of the 1.8–3.5 μm diameter particles at Long Beach.

Moving toward the smallest particles examined at Long Beach in the 0.56–1.0 μm aerodynamic diameter range, the abundance of largely unreacted sodium-containing particles falls to 3% and the carbon-containing particle population increases dramatically. Seventy-nine percent of these smaller particles produce spectra containing at least some organic and/or elemental carbon markers, possibly due to fresh primary emissions from combustion sources in Long Beach. Most of the submicron particles at Long Beach contain spectra showing mixtures of carbon and other substances, including carbon with reacted or unreacted marine aerosol (12%) and carbon with ammonium nitrate (34%). Although we believe that ammonium sulfate particles are present in this air mass on the basis of impactor sampling at Santa Catalina Island and Long Beach, these particles are not quantified in Figure 8. Negative ion mass spectra contain markers for ammonium sulfate that could be used in future

studies; however, the data set for the present experiment contained only positive ion mass spectra. Ammonium ion could be detected, but no positive ion markers for sulfate were available.

As was shown in Figures 3−5, there is a substantial increase in suspended particle mass between Long Beach and Riverside that occurs due to the emission of new particles into the air parcel as the air is transported across the basin and as atmospheric reaction products are added to individual particles. By the time that trajectory 1 reaches Riverside on the afternoon of September 24, the EAA, OPC, and ATOFMS data all indicate that the aerosol population has increased in number. The character of the particles has been greatly transformed, as can be seen by comparing the two left columns of Figure 8. During transport from Long Beach to Riverside, the percentage of the particles in the largest sizes that contain sodium has fallen and the number of complex particles containing more than two marker substances has increased. In the submicron particle sizes, transport from Long Beach to Riverside is accompanied by accumulation of complex transformed particles that contain ammonium, nitrate, and either primary or secondary carbonaceous material in amounts exceeding the quantification limits used here.

The right two columns of Figure 8 document the transformation of the particle population along trajectory 2 over the period from the morning of September 24 to the afternoon of September 25. As was noted earlier when discussing the filter and impactor data, the aerosol observed at Long Beach on September 24 shows a greater influence from urban emissions sources than the aerosol observed on the morning of September 23. The ATOFMS data show this as well, indicating that the aerosol as trajectory 2 passed over Long Beach included more carbon-containing particles, more ammonium-containing particles, and greater conversion of NaCl to $NaNO_3$ than was the case as trajectory 1 passed over Long Beach. For that reason, the relative composition of the aerosol population changes less along trajectory 2 than along trajectory 1 as the aerosol is advected from Long Beach to Riverside.

Acknowledgments

The Caltech portion of this work was sponsored by the U.S. Environmental Protection Agency Center on Airborne Organics under Grant R824970-01-0 and by the Center for Air Quality Analysis at Caltech. The UC-Riverside portion of this work was sponsored by California Air Resources Board under Contract 95-305. Thanks to Joe Cassmassi and the staff of the South Coast Air Quality Management District for providing meteorological support for these experiments. Aerosol carbon analyses were performed by Bob Cary at Sunset Laboratory, Inc., Forest Grove, OR. INAA analyses were performed by Drs. Ilhan Olmez, Michael Ames, and Jec Gone at the Nuclear Reactor Laboratory, Massachusetts Institute of Technology. We thank J. Richard Williams and Michael Berg at California State University at Long Beach and Robert Gill at California State University at Fullerton for assistance in obtaining use of the measurement sites at Long Beach and Fullerton, respectively.

Literature Cited

(1) Hughes, L. S.; Allen, J. O.; Kleeman, M. J.; Johnson, R. J.; Cass, G. R.; Gross, D. S.; Gard, E. E.; Gälli, M. E.; Morrical, B. D.; Fergenson, D. P.; Dienes, T.; Noble, C. A.; Liu, D.-Y.; Silva, P. J.; Prather, K. A. *Environ. Sci. Technol.* **1999**, *33*, 3506−3515.
(2) Roberts, P. T. Ph.D. Thesis, California Institute of Technology, 1975.
(3) Russell, A. G.; McRae, G. J.; Cass, G. R. *Atmos. Environ.* **1983**, *17*, 949−964.
(4) Reynolds, R.; Tsou, G.; Holmes, J. *The influence of gas-phase ammonia on the formation of aerosol*; Technical report; California Air Resources Board: El Monte, CA, 1975.
(5) Russell, A. G.; Cass, G. R. *Atmos. Environ.* **1986**, *20*, 2011−2025.
(6) Russell, A. G.; Cass, G. R. *Atmos. Environ.* **1984**, *18*, 1815−1827.
(7) Pandis, S. N.; Seinfeld, J. H. *Atmos. Environ.* **1992**, *26A*, 2509−2522.
(8) Lawson, D. R. *J. Air Waste Manage. Assoc.* **1990**, *40*, 156−165.
(9) Seigneur, C.; Wegrecki, A. M. *Atmos. Environ.* **1990**, *24A*, 989−1006.
(10) Richards, L. W.; Anderson, D. J.; Blumenthal, J. A.; McDonald, G. L.; Kok, A. L. *Atmos. Environ.* **1983**, *17*, 911−914.
(11) Richards, L. W. *Atmos. Environ.* **1995**, *29*, 27−46.
(12) Pandis, S. N.; Harley, R. A.; Cass, G. R.; Seinfeld, J. H. *Atmos. Environ.* **1992**, *26A*, 2269−2282.
(13) Pandis, S. N.; Wexler, A. S.; Seinfeld, J. H. *Atmos. Environ.* **1993**, *27*, 2403−2416.
(14) Eldering, A.; Cass, G. R. *J. Geophys. Res. A* **1996**, *101*, 19343−19369.
(15) Kleeman, M. J.; Cass, G. R.; Eldering, A. *J. Geophys. Res.* **1997**, *102*, 21355−21372.
(16) Pilinis, C.; Seinfeld, J. H.; Seigneur, C. *Atmos. Environ.* **1987**, *21*, 943−955.
(17) Kleeman, M. J.; Cass, G. R. *Atmos. Environ.* **1998**, *32*, 2803−2816.
(18) Wall, S. M.; John, W.; Ondo, J. L. *Atmos. Environ.* **1988**, *22*, 1649−1656.
(19) Zhang, X. Q.; McMurry, P. H.; Hering, S. V.; Casuccio, G. S. *Atmos. Environ.* **1993**, *27A*, 1593−1607.
(20) Noble, C. A.; Prather, K. A. *Environ. Sci. Technol.* **1996**, *30*, 2667−2680.
(21) Gard, E. E.; Mayer, J. E.; Morrical, B. D.; Dienes, T.; Fergenson, D. P.; Prather, K. A. *Anal. Chem.* **1997**, *69*, 4083−4091.
(22) Allen, J. O.; Hughes, L. S.; Kleeman, M. J.; Cass, G. R.; Gard, E. E.; Gross, D. S.; Galli, M. E.; Morrical, B. D.; Prather, K. A. *Environ. Sci. Technol.* **2000**, *34*, 211−217.
(23) Marple, V. A.; Rubow, K. L.; Behm, S. M. *Aerosol Sci. Technol.* **1991**, *14*, 434−446.
(24) Grosjean, E.; Grosjean, D.; Fraser, M. P.; Cass, G. R. *Environ. Sci. Technol.* **1996**, *30*, 2704−2714.
(25) Goodin, W. R.; McRae, G. J.; Seinfeld, J. H. *J. Appl. Meteorol.* **1979**, *18*, 761−771.
(26) Solomon, P. A.; Salmon, L. G.; Cass, G. R. *Environ. Sci. Technol.* **1992**, *26*, 1594−1601.
(27) Russell, A. G.; McRae, G. J.; Cass, G. R. *Atmos. Environ.* **1985**, *19*, 893−903.
(28) Hildemann, L. M.; Russell, A. G.; Cass, G. R. *Atmos. Environ.* **1984**, *18*, 1737−1750.
(29) Russell, A. G.; McCue, K. F.; Cass, G. R. *Environ. Sci. Technol.* **1988**, *22*, 1336−1347.
(30) Gray, H. A.; Cass, G. R.; Huntzicker, J. J.; Heyerdahl, E. K.; Rau, J. A. *Environ. Sci. Technol.* **1986**, *20*, 580−589.
(31) SCAQMD. *Sulfur dioxide/sulfate control study−main text*; Technical report; South Coast Air Quality Management District: El Monte, CA, 1978.
(32) Cass, G. R. *Atmos. Environ.* **1981**, *15*, 1227−1249.
(33) Fraser, M. P.; Cass, G. R. *Environ. Sci. Technol.* **1998**, *32*, 1053−1057.
(34) Russell, A. G.; McCue, K. F.; Cass, G. R. *Environ. Sci. Technol.* **1988**, *22*, 263−270.
(35) Kleeman, M. J.; Hughes, L. S.; Allen, J. O.; Cass, G. R. *Environ. Sci. Technol.* **1999**, *33*, 4331−4341.
(36) Gard, E. E.; Kleeman, M. J.; Gross, D. S.; Hughes, L. S.; Allen, J. O.; Morrical, B. D.; Fergenson, D. P.; Dienes, T.; Gaelli, M. E.; Johnson, R. J.; Cass, G. R.; Prather, K. A. *Science* **1998**, *279*, 1184−1187.
(37) Eldering, A.; Solomon, P. A.; Salmon, L. G.; Fall, T.; Cass, G. R. *Atmos. Environ.* **1991**, *25*, 2091−2102.
(38) Pio, A. C.; Harrison, R. M. *Atmos. Environ.* **1987**, *21*, 2711−2715.
(39) Ravishankara, A. R. *Science* **1997**, *276* (5315), 1058−1065.
(40) Langer, S.; Pemberton, R. S.; Finlayson-Pitts, B. J. *J. Phys. Chem. A* **1997**, *101* (7), 1277−1286.
(41) Vogt, R.; Crutzen, P. J.; Sander, R. *Nature* **1996**, *383* (6598), 327−330.
(42) Pszenny, A. A. P.; Keene, W. C.; Jacob, D. J.; Fan, S.; Maben, J. R.; Zetwo, M. P.; Springeryoung, M.; Galloway, J. N. *Geophys. Res. Lett.* **1993**, *20* (8), 699−702.
(43) Gross, D. S.; Gaelli, M. E.; Silva, P. J.; Prather, K. A. *Anal. Chem.* **2000**, *72*, 416−422.

Received for review July 28, 1999. Revised manuscript received December 10, 1999. Accepted December 23, 1999.
ES9908671